Graphical Abstract
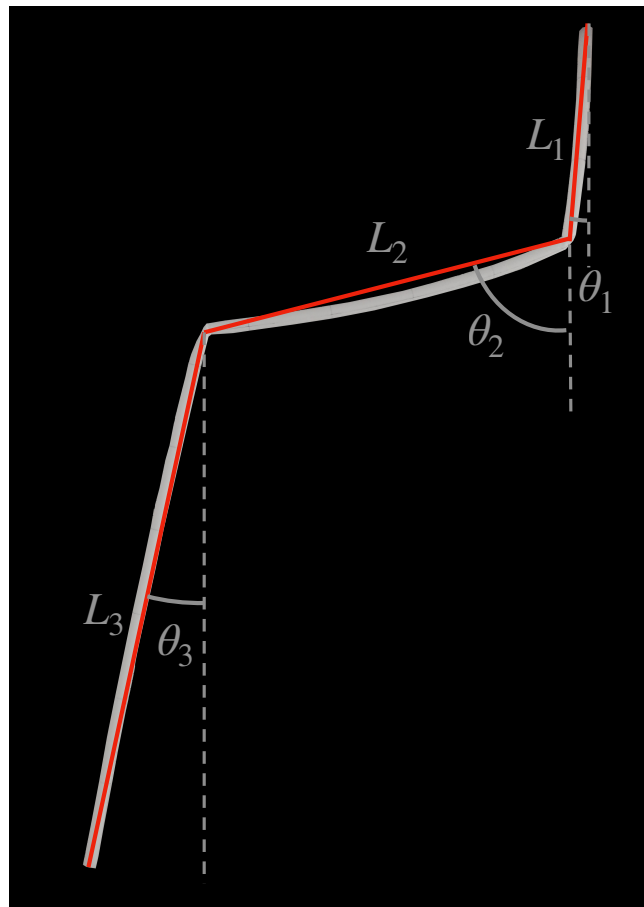
Divergence instability in an air-conveying soft tube: analysis of static zig-zag shapes

O. D. Donato Angulo, C. Eloy, A. Cros

Highlights

Divergence instability in an air-conveying soft tube: analysis of static zig-zag shapes

O. D. Donato Angulo, C. Eloy, A. Cros

- an air-conveying, hanging soft tube exhibits stable zig-zag states

- not all configurations for the zig-zag states are allowed

- a model of three articulated rigid tubes connected by torsional springs reproduce the same kind of stable states

Divergence instability in an air-conveying soft tube: analysis of static zig-zag shapes

O. D. Donato Angulo[a], C. Eloy[b], A. Cros[a,*]

[a]*Physics Department, Universidad de Guadalajara, Blvd. Gral. Marcelino García Barragán 1421, Olímpica, 44430 Guadalajara, Jalisco, México*
[b]*Aix Marseille Univ, CNRS, Centrale Marseille, IRPHE, Marseille, France*

Abstract

This work is devoted to the characterization and modeling of surprising stable states appearing in air-conveying soft tubes. A soft tube differs from a flexible tube by its very thin walls which allows it to fold with a sharp angle. When the upper end of a soft tube is fixed to an air pump while the bottom end is left free, the system exhibits a divergence instability which develops under the form of "zig-zag" shapes constituted by three roughly straight segments. We characterize each stable shape by the lengths and angles of these three segments. We observe, for example, that the intermediate segment is limited to short lengths because its inclined direction with respect to the vertical increases the gravitational torque on the upper fold. In order to theoretically reproduce the zig-zag shapes, we use a model of three articulated straight rigid tubes conveying airflow. The torque exerted by the pressurized tube on a folded part of the pipe is modeled by a nonlinear torsional spring. This model shows that the system can stabilize into zig-zag states qualitatively similar to experimental observations.

Keywords: Fluid-structure interaction, cantilever soft tube, divergence

1. Introduction

An aeroelastic instability is at the origin of the spontaneous fluctuations of a cantilevered, flexible tube which conveys a fluid with a high enough velocity

---

(Païdoussis, 1998; Fung, 2008; Bisplinghoff et al., 2013; Huvelin et al., 2007). In 1966, Gregory and Païdoussis (1966a,b) established the motion equation for horizontal, flexible tubes which convey a flow from their fixed end to their free extreme. These authors established the critical velocity at which the tubes spontaneously fluctuate as well as their oscillation frequency. A few years later, Païdoussis (1970) considered gravity effects in his stability analysis of a hanging, horizontal or standing, flexible tube. In this case, the critical nondimensional flow velocity above which fluctuations occur depends upon two nondimensional numbers: the ratio β of the fluid mass over the whole system mass, and the number γ which represents the gravity effects divided by the rigidity effects. As expected, the critical velocity is higher for hanging cantilevers than for standing cantilevers.

The same instability was discovered a few years before by Benjamin (1962b,a) who established the stability conditions for a system of n articulated rigid pipes through which an incompressible fluid flows. The tubes are connected by elastic joints and submitted to planar motions. When the inlet is fixed at the system upper extreme while the outlet is left free, two kinds of instabilities were observed with water: the amplified vibrations as for flexible tubes, and divergence. This latter, also called "buckling", stands for a static instability and corresponds to a deflected shape of the discrete system. Benjamin (1962b) showed that gravity is a necessary ingredient for the buckling to occur and that, moreover, this phenomenon is allowed only for specific ranges of the parameter β. This is why divergence did not appear in his experiments with airflow. This latter result was recently confirmed by Schouveiler and Chermette (2018) who found that divergence only occurs for great values of β.

Since an infinite number of connected rigid tubes tends to the case of a flexible tube, both systems should exhibit the same instabilities. Nevertheless, Païdoussis (1970); Benjamin (1962b); Handelman (1955) reported that buckling could not develop for a flexible tube. This paradox was solved by Païdoussis and Deksnis (1970) who found that divergence is associated to the higher modes of the discrete system which are different from those of the continuous system.

A way to "activate" the buckling instability without changing the value of β in an articulated system composed by two segments was found by Bohn and Herrmann (1974). In this study, the second tube was allowed to oscillate in a plane different from the oscillation plane of the upper pipe such that the system is characterized by a new parameter α. They found that, when the

2

two planes are perpendicular ($\alpha = 90°$), the system becomes unstable via divergence. For angles $0° < \alpha < 90°$, the system can lose its stability either by fluttering either by buckling depending upon the other parameters.

Three-dimensional motions were taken into account for flexible pipes by Bajaj and Sethna (1984); Modarres-Sadeghi et al. (2008); Wang et al. (2018) who proposed more complex motion equations than in 2D and plotted modified stability curves. Experimentally, this kind of motions are unavoidable in air-conveying, thin-walled tubes. This is the case of the "sky dancers" which are long, vertical fabric-made tubes which fluctuate above an air blower in order to advertise a product: for high enough airflow, the fluctuations may be very disordered. In such systems, contrarily to flexible tubes, sharp angles appear along the tube. Flores-Castillo and Cros (2009) reproduced a reduced model of sky dancer in their laboratory and described how a fold propagates along the soft tube as it is pushed away from the pump exit thanks to the air pressure. Moreover, the critical velocity above which the sky dancer fluctuates (Cros et al., 2012) is higher than the predicted value by Païdoussis (1970) ; this result suggests that a different mechanism is involved in the sky dancer stability. Finally, Orozco-Estrada et al. (2020) analyzed the intermittent regime which develops. When the soft tube is fixed by its upper extreme indeed, the fluctuations may be interrupted by long, static states during which the tube exhibits a stable, zig-zag shape.

The purpose of this study is to characterize these static zig-zag states and to model them with a theoretical model. Section 2 is devoted to the experimental device description while the results are reported in Section 3. The model presented in Section 4 allows to reproduce the same kind of zig-zag states for a part of the phase diagram. Section 5 concludes this study.

2. Experimental device

The experimental device is shown in Fig. 1. The air blower is a centrifugal pump (model Pasco SF-9216) whose electric power can be varied as described in Orozco-Estrada et al. (2020). For low electric power values, the tube remains vertical and static, while for high values the tube always fluctuates. In the present work, the pump power is fixed to an intermediate value in such a way that static states alternate with chaotic fluctuations. In this case, the pump characteristic curve is drawn in Fig. 2. The left vertical axis corresponds to the volumetric flow rate Q while the right vertical axis is the associated air velocity v if the tube was considered rigid.
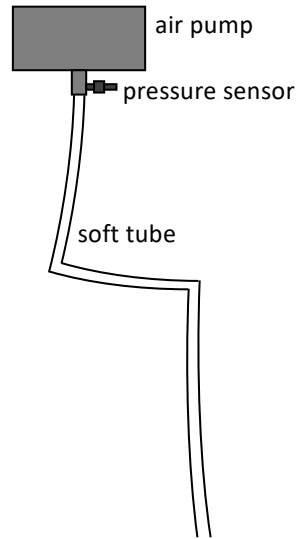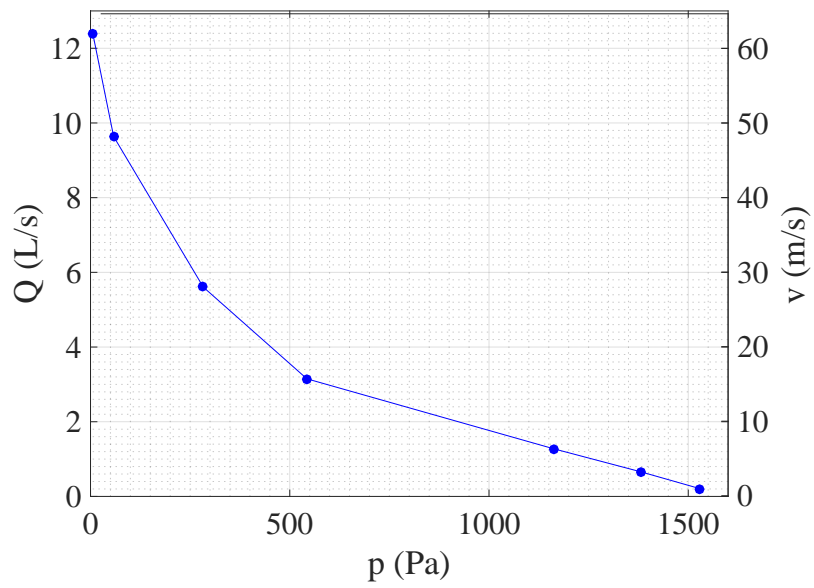
Figure 1: Experimental set-up.

Figure 2: Characteristic curve of the centrifugal pump.

Table 1: Tube characteristics: L is its length, $2R$ its diameter, m_t is the tube mass per unit of length.

L (cm)	$2R$ (cm)	m_t (g/m)
136.0 ± 0.2	1.6 ± 0.1	4.2 ± 0.1

The tube characteristics are given in Table 1. The soft tubes are made by heat-sealing a plastic fabric over its whole length. A pressure sensor connected to the pump outlet (Burster 8227-4100-V134) permits to measure the differential pressure when a static state is reached. Then the air velocity can be deduced by taking into account the characteristic curve (Fig. 2).

The static states are analized as following. First, the soft tube vertically hangs from the blower exit and begins to fluctuate as soon as the pump is switched on. If the system evolves without any external intervention, after a more or less long time (from a few seconds to several minutes) the tube always reaches a static state (Orozco-Estrada et al., 2020). The stable states are systematically identified by three roughly straight portions separated by sharp angles as shown in Fig. 3. The experimenter may take a picture or directly measure the different segment lengths, the angles of each tube portion with respect to the vertical direction and the pressure at the tube inlet. These parameters are shown in Fig. 3.

Now, in order to explore the greatest set of possible stable states, the experimenter interferes by maintaining different positions of the tube and releasing them. If the tube keeps static, the corresponding state is recorded. In the case that the system is unstable, another position is tried. A systematic exploration of the lengths is performed by hand-fixing a first point of the tube below the pump simultaneously to a second point below. Both points are moved away from their rest positions with different angles and the stability of the configuration is easily estimated. The lengths are modified by 10 cm and the same procedure is repeated.

3. Experimental static states

Some stable state photographs are shown in Fig. 4. The most inclined segment with respect to the vertical direction is always the middle tube portion. The upper segment is generally slightly curved and the angle θ_1 is identified by fitting a straight line from the pump exit to the first fold.
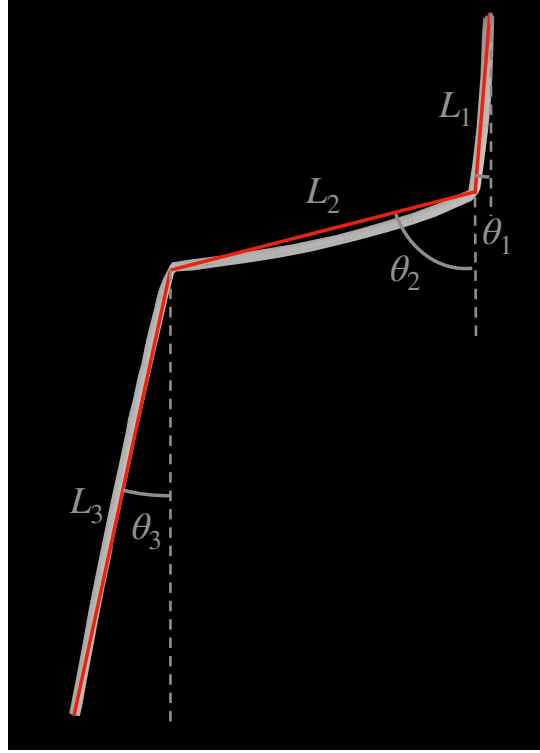
Figure 3: Illustration of the 6 parameters which identify a stable state. The soft tube becomes stable by forming a zig-zag shape constituted of three roughly straight tube portions shown in white in this figure. The red straight lines indicate the approximation made in order to characterize the following parameters. The upper segment length is noted L_1, while L_2 and L_3 denote the lengths of the intermediate and bottom segments, respectively. Moreover, θ_1, θ_2 and θ_3 are the angles of each segment with respect to the vertical direction. For this profile, $L_1 = 0.19\,L_{tot}$, $L_2 = 0.33\,L_{tot}$, $L_3 = 0.48\,L_{tot}$. In this figure, all the angles are negative.

Figure 5 shows the state diagram in the plane $(L_1/L_{tot},\ L_2/L_{tot})$. The length of the bottom tube segment can be deduced from $L_3 = L_{tot} - (L_1 + L_2)$. Each stable state is represented by a square whose width represents the ± 1.4 cm errorbar. It can be observed that, while the upper segment reaches lengths $0 < L_1 < 0.79\,L_{tot}$, the intermediate segment is limited to shorter lengths since $L_2 < 0.41\,L_{tot}$. Indeed, the angle θ_2 of this tube portion is bigger than the other two angles θ_1 and θ_3 so that the potential energy is increased and the weight supported by this tube portion cannot be too high. The bottom segment interval is $0.10\,L_{tot} < L_3 < 0.74\,L_{tot}$.

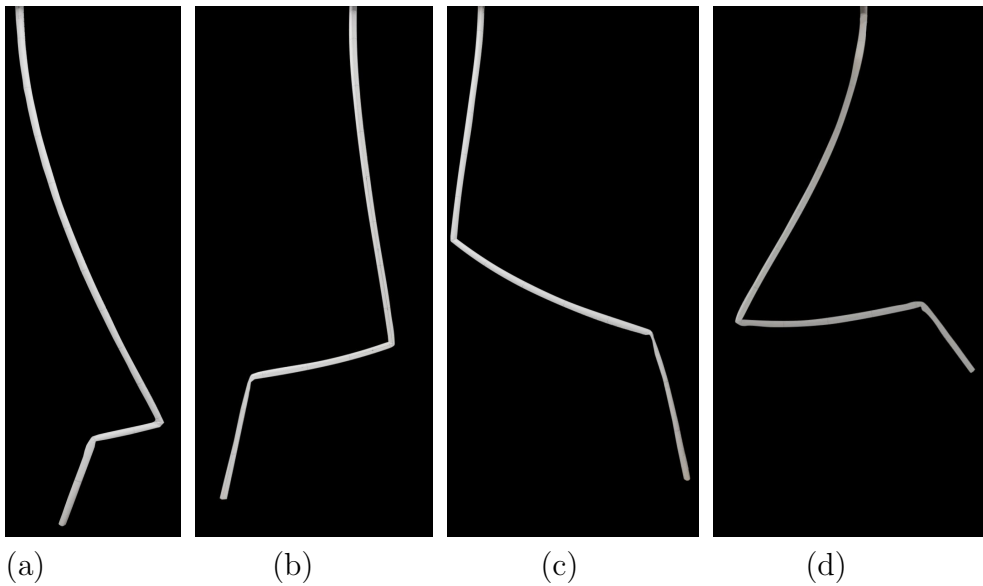(a)   (b)   (c)   (d)

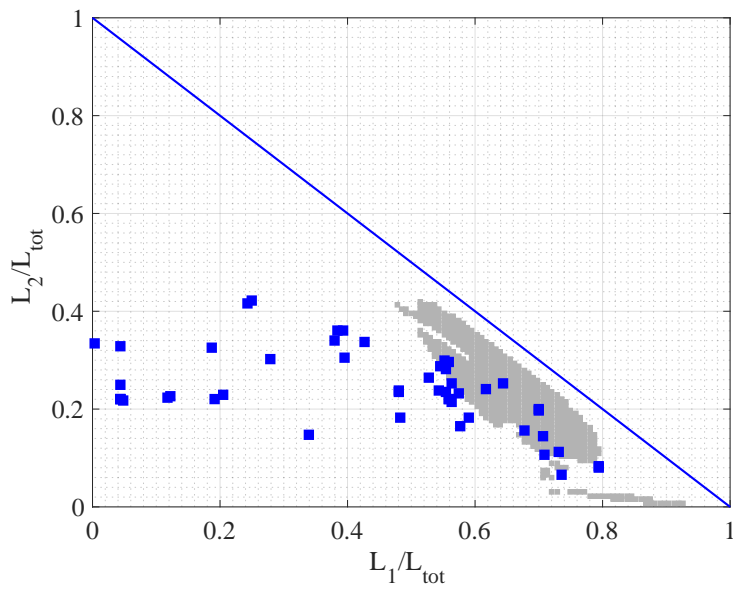Figure 4: Photographs of stable states. The height of all these images is 130 cm.

Figure 5: State diagram of the stable states. Each blue squared symbol represents a stable state with an errorbar of ± 0.01. The line from $(1; 0)$ to $(0; 1)$ delimits the possible values of $L_1/L_{tot} + L_2/L_{tot} < 1$. The gray area corresponds to the stable region found by the theoretical model for $\kappa = 1.7 \times 10^{-4}$ N·m and $U = 10$ m/s (see Section 4.3).
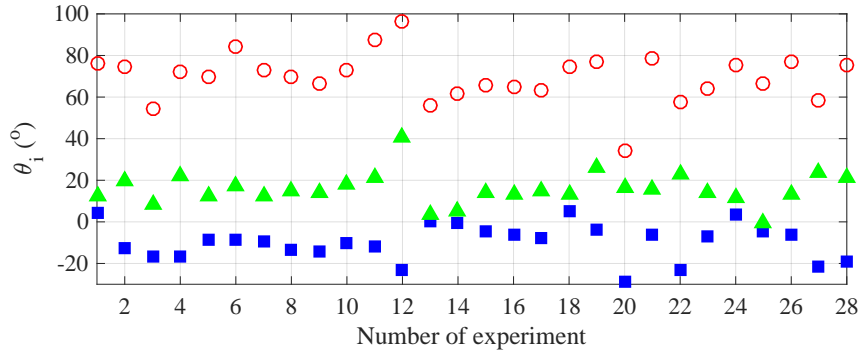
Figure 6: θ_i values for different experiments. (■) θ_1, (o) θ_2, (▲) θ_3.

Typical angle values are shown in Fig. 6. To make it clearer, we considered for all the static states $\theta_3 > 0$ and the signs of the other two angles are deduced: that is to say that we horizontally flip the zig-zag shape photographies like Fig. 4(a) and (b). As expected, the first angle is small $(-30° < \theta_1 < 5°)$ since higher values would be very expensive in potential energy. The angle θ_2 has got the greatest value $(33° < \theta_2 < 95°)$ while $0° < \theta_3 < 40°$. A striking behaviour is that in the most stable shapes, the sign of θ_1 is opposite to the sign of the two other angles.

4. Model

4.1. Description

In order to better understand the static shapes observed, we model the flexible pipe by a system of 3 articulated rigid pipes connected by torsional springs (Fig. 7). We use the framework of Lagrangian mechanics and we follow the derivation of Benjamin (Benjamin, 1962b), which we shall briefly recall.

The Lagrangian of the system, $\mathscr{L}$, is decomposed into three terms $\mathcal{L}_i$ with $i = \{, 1; 2; 3\}$, corresponding to the Lagrangians of each rigid tube i. The individual Lagrangians can be written as $\mathcal{L}_i = T_i - V_i$, where T_i is the the kinetic energy of segment i due to both the fluid and the solid kinetic energies, whereas V_i is the potential energy, which has two components: the fluid and the solid gravitational energies and the torsional spring energy.
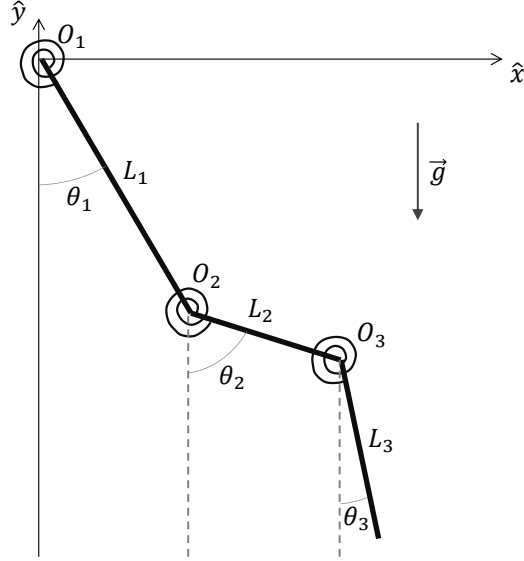
8

Figure 7: Model.

The system dynamics is then governed by the Euler–Lagrange equations

$$\frac{d}{dt}\left(\frac{\partial \mathscr{L}}{\partial \dot{q}_i}\right) - \frac{\partial \mathscr{L}}{\partial q_i} = -m_f U\left(\dot{\mathbf{R}} + U\hat{\mathbf{e}}_{\mathbf{t}}\right) \cdot \frac{\partial \mathbf{R}}{\partial q_i} \quad \text{with } \mathscr{L} = \sum_{i=1}^{3} \mathcal{L}_i, \quad (1)$$

with q_i the generalized coordinates, which in this case are simply the angles θ_i between the segments and the vertical. In the above Euler–Lagrange equations, the right-hand side is a generalized force due to the fluid flow, where $\mathbf{R}$ is the position of the free-end and $\hat{\mathbf{e}}_{\mathbf{t}}$ is a unit vector oriented in the direction of the last segment. The Euler-Lagrange (Eqs. 1) form a system of ordinary differential equations that are integrated numerically using an order-2 Runge-Kutta scheme (the function ode23 in Matlab).

4.2. Potential

The torsional springs model the torque that the pressurized pipe exerts on a fold (Fig. 7). These folds involving complex non-linearities, they are difficult to model and are probably different from a soft tube to another. We choose to model the torque through a function as simple as possible with

9

three properties: (1) it is linear for small angles θ, (2) it is even and (3) when $\theta \to \pi$, the torque diverges, which is necessary to avoid angles greater than π. Although alternative choices would be possible, we choose the following function for the torque:

$$\tau(\theta) = \kappa \frac{\pi^2 \theta}{\pi^2 - \theta^2} \ , \tag{2}$$

where κ is a spring constant that will be measured with dedicated experiments. The function $\tau(\theta)$ is easily integrable, so that the corresponding potential is:

$$V(\theta) = -\frac{\pi^2}{2} \kappa \log\left(\frac{\pi^2 - \theta^2}{\pi^2}\right) \ . \tag{3}$$

In order to estimate a value for κ, we performed the following experiments. The tube free end is partially sealed to control the pressure while the other end is clamped onto the pump exit. We then incline the pump exit by an angle α as shown in Fig. 8(a) and the tube is folded in order to let a ℓ-long portion hang (see Fig. 8b).

At equilibrium, the torque exerted by the airflow onto the fold balances the torque due to the weight of the hanging portion: $\tau = \frac{1}{2} m_t g \ell^2 \sin \theta$. With this method, we can estimate the torque exerted onto a fold for a range of angles θ ($90° < \theta < 150°$). Note that when the tube is pressurized the low values of θ are impossible to reach because, in that case, the tube spontaneously unfolds.

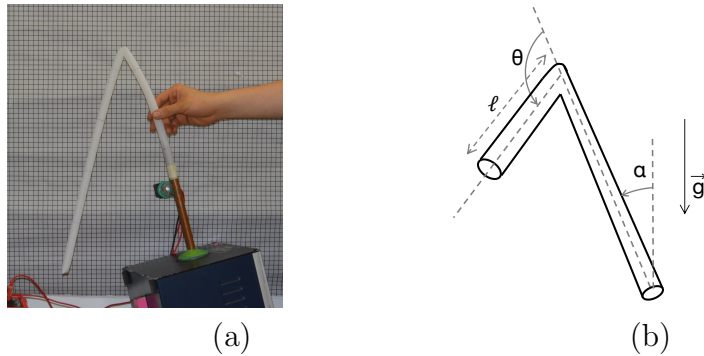(a)   (b)

Figure 8: (a) Photograph of the experiment performed to estimate the torque. The soft tube is pressurized by connecting it to the pump. The hanging length ℓ and the angle θ shown in (b) permit to deduce the experimental torque.
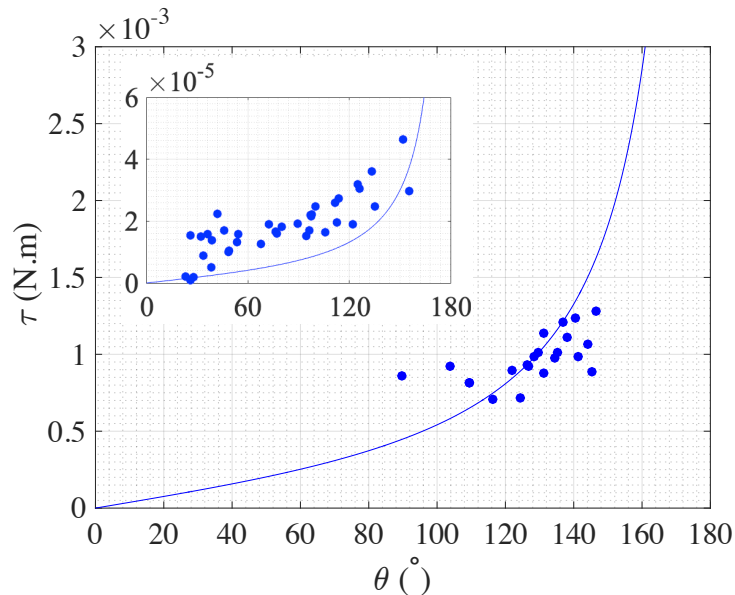
10

Figure 9: Estimation of the torque exerted by the tube on a segment, as a function of the angle. The main plot shows the results for the pressurized tube while the inset corresponds to the torque of the tube without airflow. The lines show the model, Eq. (2), with $\kappa = 1.7 \times 10^{-4}$ N·m for the pressurized tube and $\kappa = 3.5 \times 10^{-6}$ N·m for the tube without airflow.

Figure 9 shows the measurements of the torque and the fit by the function given in Eq. 2 for two cases: a pressurized tube and a tube without airflow. The resulting fitted spring constant differs by two orders of magnitude, showing the importance of the pressure forces in this complex and highly nonlinear fluid-structure interaction. In the following, we will use Eq. 2 with the spring constant κ found for pressurized tubes to model the system. Note that if we use the value of κ for tubes with no airflow, the zig-zag states are unstable.

4.3. Results

Using Eq. 3 to define the Lagrangian of the system and using the Euler-Lagrange equations written in Eq. 1 allows us to simulate the dynamics of the system. To identify the region of the parameter space where stable zig-zag states exist, we use the following methodology. All the parameters $L_1, L_2, L_3, L_{tot}, U$ as well as the initial angles $\theta_i(0)$ are fixed. Then the evolutions of $\theta_{i,\{i=1;2;3\}}(t)$ are simulated.

11

As explained in Section 4.2, when $U = 10$ m/s and $\kappa = 3.5 \times 10^{-6}$ N·m, the tubes always remain in a vertical position. When $U = 10$ m/s and $\kappa = 1.7 \times 10^{-4}$ N·m however, five different regimes can be observed, four of them being illustrated in Fig. 10. In regime (1), the system exhibits damped oscillations that converge to a vertical straight shape (Fig. 10a). In regime (2), the articulated tubes exhibit finite and sustained oscillations around the vertical (Fig. 10b). In regime (3), the system reaches a steady state different from the vertical (Fig. 10c): this is the stable zig-zag state. In regime (4), each tube oscillates around a zig-zag configuration (Fig. 10d). Finally, regime (5) is associated to an unstable and chaotic behavior of the system.
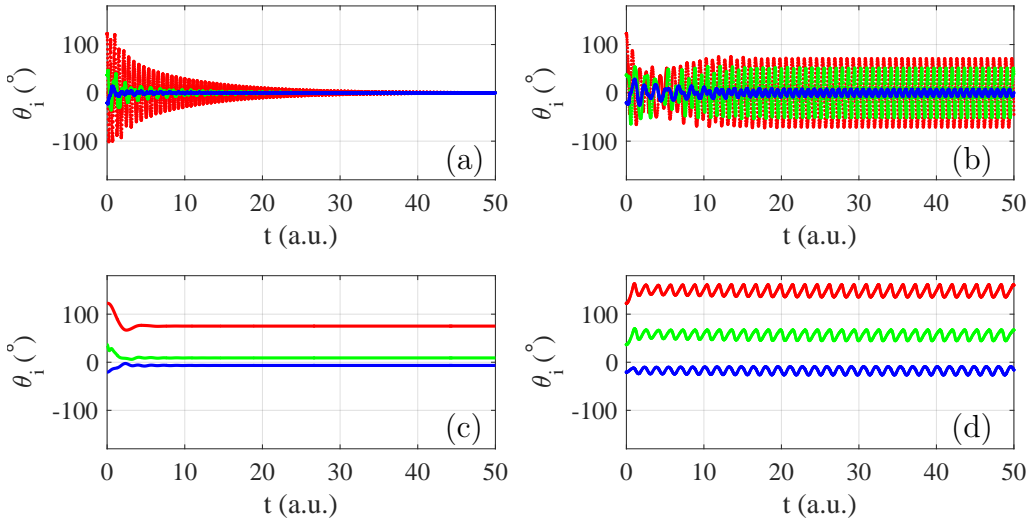

Figure 10: Theoretical angle temporal evolution for $U = 10$ m/s, $\kappa = 1.7 \times 10^{-4}$ N·m and $L_1 = 0.552\,L_{tot}$ for: (a) $L_2 = 0.050\,L_{tot}$, (b) $L_2 = 0.120\,L_{tot}$, (c) $L_2 = 0.300\,L_{tot}$ and (d) $L_2 = 0.320\,L_{tot}$. Blue curves are for θ_1, red cruves for θ_2 and green ones for θ_3.

Case (3) corresponds to a stable zig-zag state and its region of existence for $U = 10$ m/s and $\kappa = 1.7 \times 10^{-4}$ N·m for different L_1/L_{tot} and L_2/L_{tot} values is identified by the gray area in Fig. 5. We observe that theoretical stable zig-zag shapes can develop only for large enough L_1 values ($L_1 \geq 0.478\,L_{tot}$). Additionnaly to the connex region around ($L_1/L_{tot} \sim 0.65$, $L_2/L_{tot} \sim 0.25$), a thin line of stable states was found around ($L_2/L_{tot} \sim 0.02$; $0.75 \lesssim L_1/L_{tot} \lesssim 0.93$).

In order to better understand the form of the theoretical state diagram, we

characterize the solutions found for a vertical line of Fig. 5 at $L_1/L_{tot} = 0.552$. For this fixed value, Fig. 11 shows the evolution of the angles as a function of L_2/L_{tot}. In this plot, the symbols show the mean angles and the errorbars show the oscillation amplitude around these means.
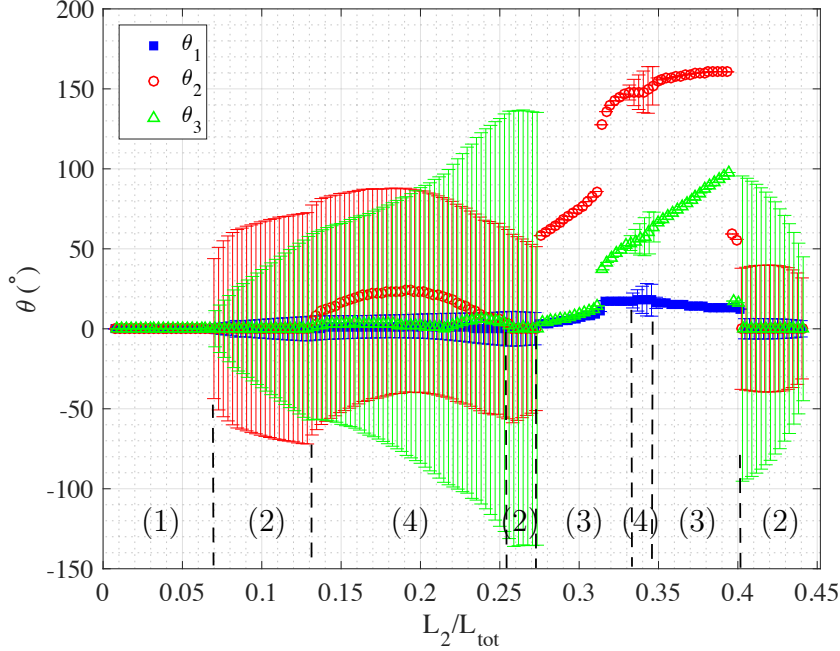

Figure 11: Evolution of the equilibrium angles for $U = 10$ m/s, $\kappa_0 = 1.7 \times 10^{-4}$ N·m and $L_1 = 0.552\,L_{tot}$ as a function of L_2/L_{tot}. Symbols show mean values of θ_1, θ_2 and θ_3 and errorbars show the amplitude of oscillations. The labels indicate the different regimes: (1) stable ; (2) oscillations around the vertical ; (3) zig-zag ; (4) oscillations around zig-zag.

For $L_2/L_{tot} < 0.067$, the system is vertical (regime 1), as seen in Fig. 11. For larger values of $L2$ ($0.067 < L_2/L_{tot} < 0.274$), this static equilibrium becomes unstable and the system oscillates around the vertical (regime 2). Inside this interval for L_2, the mean value of angle θ_2 is no longer zero (for $0.131 < L_2/L_{tot} < 0.256$): this corresponds to regime (4). For $0.274 < L_2/L_{tot} < 0.402$, the system exhibits a stable zig-zag (regime 3), except in a small interval ($0.274 < L_2/L_{tot} < 0.348$), which corresponds to small oscillations around the zigzag state (regime 4). For $0.402 < L_2/L_{tot} < 0.441$, the system is in regime (2) again. For larger values, $L_2 > 0.441$, the system is chaotic (regime 5): the segments may perform several rotations around

13

their articulations and never stabilize. This analysis shows that the system of articulated tubes may exhibit a wide range of behaviors that depends on the segment lengths. We will now focus on the stable zig-zag states (regime 3).

In order to assess the influence of the spring constant, we plotted in Fig. 12 the points for which the system exhibits stable zig-zag states for three values of the spring constant: $\kappa_0 = 1.7 \times 10^{-4}$ N·m, $\kappa = 0.9\,\kappa_0$ and $\kappa = 1.1\,\kappa_0$. We find that when κ is lower by 10%, these profiles develop for slighly larger L_1 values and the unstable (regime (4)) strip from (0.51; 0.37) to (0.58; 0.31) is larger. So it seems that a lower κ value destabilizes the system. On the contrary, a higher κ value allows to convert the unstable strip into a stable one (regime (3)).

The evolution of the values of θ_i when the system has reached its equilibrium as a function of U is shown in Fig. 13(b) for fixed values of L_i and for
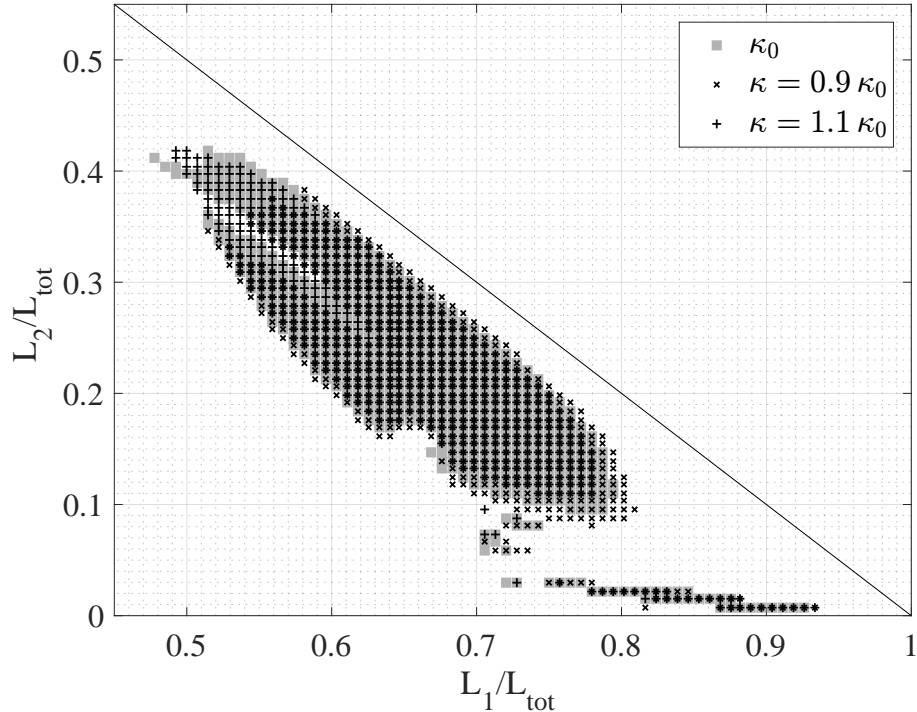

Figure 12: Comparison of stable zig-zag states found with $U = 10$ m/s, (■) $\kappa_0 = 1.7 \times 10^{-4}$ N·m, (+) $\kappa = 1.1\,\kappa_0$, (×) $\kappa = 0.9\,\kappa_0$.
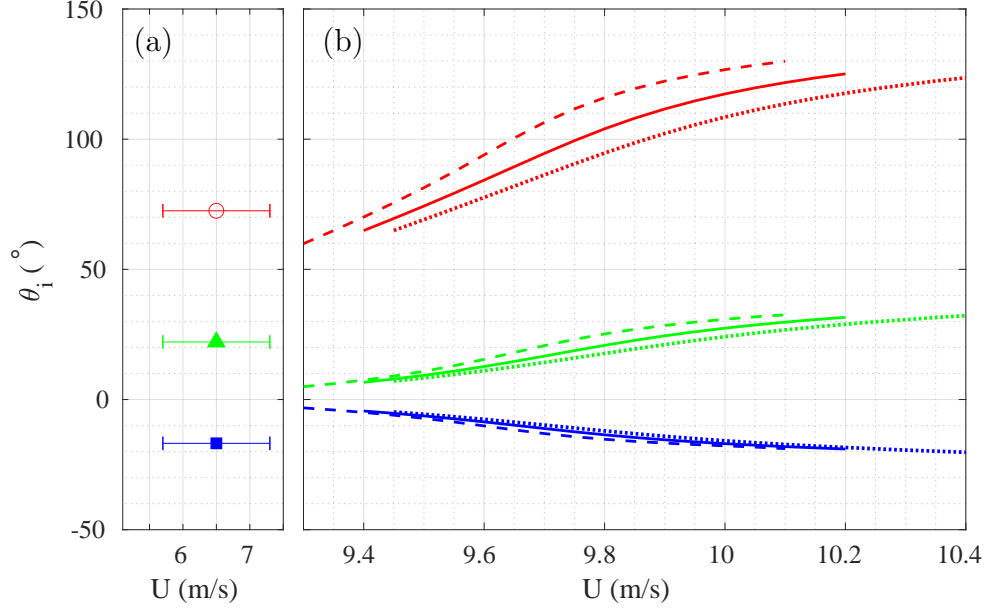
14

Figure 13: a) Experimental data for the same L_1 and L_2 values as in (b) for experiment #4 of Fig. 6, as a function of its estimated velocity. b) Theoretical evolution of the angles for $L_1 = 0.616\,L_{tot}$, $L_2 = 0.241\,L_{tot}$ as the air velocity U is varied. The blue curves stand or θ_1, red ones for θ_2 and green ones for θ_3. The plain lines show the results for $\kappa_0 = 1.7 \times 10^{-4}$ N·m, dashed lines for $\kappa = 0.9\,\kappa_0$, dotted lines for $\kappa = 1.1\,\kappa_0$.
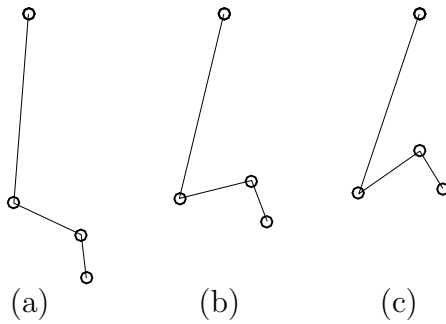

Figure 14: Illustration of the theoretical stable shapes of the system of three articulated tubes for $L_1 = 0.616\,L_{tot}$, $L_2 = 0.241\,L_{tot}$, $\kappa_0 = 1.7 \times 10^{-4}$ N·m and (a) $U = 9.2$ m/s, (b) 9.8 m/s and (c) 10.2 m/s.

15

adapted velocity intervals which depend upon the κ value. Outside these intervals, the system does not exhibit stable zig-zag shapes. As an illustration the tube profiles for $U = 9.4$; 9.8 and 10.2 m/s are shown in Fig. 14. It can be seen that, like in experiments (Fig. 6), θ_1 has an opposite sign compared to θ_2 and θ_3 and the intermediate segment is more inclined that the upper and the bottom segments. Moreover, a change in the spring constant (dashed and dotted lines in Fig. 13(b)) modifies the velocity interval for which stable zig-zag shapes develop: this interval tends to lower velocity values when κ is decreased and to upper U values when κ is increased. For a given airflow, the angles are greater when the spring constant is lower, as expected. Finally, as a comparison, the angle values of our experiment # 4 are shown in Fig. 13(a) since for this experiment the segment lengths are the same as in Fig. 13(b).

Let note that the pump characteristic curve permits to associate the pressure values measured for each zig-zag shape to the air velocity: we found $U \simeq [5; 8]$ m/s for the experimental points shown in Fig. 5 and $U = 6.5 \pm 0.8$ m/s for experiment # 4 of Fig. 13(a). This value is lower than the velocity range of Fig. 13(b) for which stable zig-zag profiles exist, but the real velocity in the folds should be greater because of the reduced cross section when the tube folds. Moreover, the experimental velocity interval is of the same order of magnitude of the velocity interval shown by Fig. 13.

We recall that the region of theoretically stable zig-zag states has been reported in the experimental phase diagram of Fig. 5 as a gray area for $\kappa = 1.7 \times 10^{-4}$ N·m. We observe that this region does not expand as much as the experimental points, in particular for low L_1 values. However, the intermediate segment length interval is well reproduced and the angle values are qualitatively the same as in the theory. Our simplified model does not take into account the whole complexity of the experimental system ; nevertheless it allows to relate the stable zig-zag states which appear in our experiments to the presence of nonlinear torques in the soft tube folds. Because of our tube softness, the articulations are not fixed along the tube and theoretical regimes (2) and (4) were not observed in our laboratory experiment. It is beyond the scope of this study to model precisely what happens in the folds, but our experiment shows that airflow and air pressure play a crucial role together with the highly nonlinear elastic deformations.

5. Conclusion

To our knowledge, this system is the first one for which divergence is observed in a clamped-free air-conveying pipe. Without the intervention of the experimenter, the corresponding zig-zag profiles may remain stable several minutes and then destabilize into chaotic, three-dimensional fluctuations leading to an intermittent regime (Orozco-Estrada et al., 2020). This behavior suggests that the basin of attraction of the zig-zag states is very shallow. The stable states are always formed by three roughly straight portions separated by sharp angles. In the present work, we explored all the allowed static shapes. We measured the lengths of each portion as well as the angles they form with respect to the vertical direction. We found that the upper segment length spans a broad interval $0 \leq L_1/L_{tot} \leq 0.8$ while the intermediate portion has lower values : $0.06 \leq L_2/L_{tot} \leq 0.42$. This intermediate segment is also the most inclined with respect to the vertical direction and large L_2 values would exert a gravitational torque on the upper folds that tends to unfold it. The smallest angle is given by the upper segment and has an opposite sign with respect to the other two angles.

A theoretical model was implemented where three rigid articulated pipes convey air while they are connected via nonlinear torsional springs. The nonlinear spring law was chosen on the basis of theoretical considerations. The spring constant was then fitted with dedicated experiments. Our model reproduces the same kind of zig-zag, stable states as in our experiments in a region $L_1/L_{tot} \gtrsim 0.5$. This smaller interval with respect to the experimental results is explained by the simplicity of our model. The experimental nonlinearities coming from the complex interaction between the variable airflow, the soft tube, the changing cross section, the folded points and the pressure gradient along the tube are all contained into the simple nonlinear spring law in our theoretical model. Nevertheless, our basic model reproduce zig-zag states whose angles are in qualitative agreement with the experiment.

References

AK Bajaj and PR Sethna. Flow induced bifurcations to three-dimensional oscillatory motions in continuous tubes. <u>SIAM Journal on Applied Mathematics</u>, 44(2):270–286, 1984.

Thomas Brooke Benjamin. Dynamics of a system of articulated pipes conveying fluid ii. experiments. <u>Proceedings of the Royal Society of London. Series A. Mathematical and Physical Sciences</u>, 261(1307):487–499, 1962a.

Thomas Brooke Benjamin. Dynamics of a system of articulated pipes conveying fluid i. theory. <u>Proceedings of the Royal Society of London. Series A. Mathematical and Physical Sciences</u>, 261(1307):457–486, 1962b.

Raymond L Bisplinghoff, Holt Ashley, and Robert L Halfman. <u>Aeroelasticity</u>. Courier Corporation, 2013.

Michael P Bohn and George Herrmann. Instabilities of a spatial system of articulated pipes conveying fluid. Technical report, 1974.

A. Cros, J. A. Rodríguez-Romero, and F. Castillo-Flores. Sky dancer: a complex fluid-structure interaction. In <u>Experimental and Theoretical Advances in Fluid Dynamics</u>, pages 15–24. Berlin: Springer, 2012.

F Flores-Castillo and A Cros. Transition to chaos of a vertical collapsible tube conveying air flow. <u>Journal of Physics: Conference Series</u>, 166(1): 012017, 2009.

Yuan Cheng Fung. <u>An introduction to the theory of aeroelasticity</u>. Courier Dover Publications, 2008.

RW Gregory and MP Païdoussis. Unstable oscillation of tubular cantilevers conveying fluid ii. experiments. <u>Proceedings of the Royal Society of London. Series A. Mathematical and Physical Sciences</u>, 293(1435):528–542, 1966a.

RW Gregory and MP Païdoussis. Unstable oscillation of tubular cantilevers conveying fluid i. theory. <u>Proceedings of the Royal Society of London. Series A. Mathematical and Physical Sciences</u>, 293(1435):512–527, 1966b.

George H Handelman. A note on the transverse vibration of a tube containing flowing fluid. <u>Quarterly of Applied Mathematics</u>, 13(3):326–330, 1955.

Fabien Huvelin, Élisabeth Longatte, and Mhamed Souli. Simulation numérique d'un tube flexible soumis à un écoulement interne. Mechanics & Industry, 8(2):143–149, 2007.

Yahya Modarres-Sadeghi, Michael P Paı, Christian Semler, et al. Three-dimensional oscillations of a cantilever pipe conveying fluid. International Journal of Non-Linear Mechanics, 43(1):18–25, 2008.

Arturo Orozco-Estrada, Ricardo Morales-Hernández, Ricardo Lima, and Anne Cros. Multistability intermittency in an air-conveying soft tube. Communications in Nonlinear Science and Numerical Simulation, 82: 105057, 2020.

Michael P Païdoussis. Dynamics of tubular cantilevers conveying fluid. Journal of Mechanical Engineering Science, 12(2):85–103, 1970.

Michael P Païdoussis. Fluid-structure interactions: slender structures and axial flow, volume 1. Academic press, 1998.

MP Païdoussis and EB Deksnis. Articulated models of cantilevers conveying fluid: the study of a paradox. Journal of Mechanical Engineering Science, 12(4):288–300, 1970.

Lionel Schouveiler and Félix Chermette. Flutter instability of freely hanging articulated pipes conveying fluid. Physics of Fluids, 30(3):034105, 2018.

Yikun Wang, Lin Wang, Qiao Ni, Huliang Dai, Hao Yan, and Yangyang Luo. Non-planar responses of cantilevered pipes conveying fluid with intermediate motion constraints. Nonlinear Dynamics, 93(2):505–524, 2018.